



Simultaneous bioimaging recognition of cation Al^{3+} and anion F^- by a fluorogenic method



Yong Sung Kim^{a, b}, Jae Jun Lee^{a, b, **}, Ye Won Choi^{a, b}, Ga Rim You^{a, b}, LeTuyen Nguyen^c, Insup Noh^c, Cheal Kim^{a, b, *}

^a Department of Fine Chemistry, Seoul National University of Science and Technology, Seoul 139-743, Republic of Korea

^b Department of Interdisciplinary Bio IT Materials, Seoul National University of Science and Technology, Seoul 139-743, Republic of Korea

^c Department of Chemical and Biomolecular Engineering, and Convergence Program of Biomedical Engineering and Biomaterials, Seoul National University of Science & Technology, Seoul 139-743, Republic of Korea

ARTICLE INFO

Article history:

Received 28 November 2015

Received in revised form

26 January 2016

Accepted 8 February 2016

Available online 23 February 2016

Keywords:

Fluorescence

Julolidine

Aluminum ion

Fluoride

Cell imaging

Theoretical calculations

ABSTRACT

A new highly selective and sensitive chemosensor **1** for both Al^{3+} and F^- was designed and synthesized. **1** could detect both Al^{3+} and F^- with turn-on fluorescence behavior in a nearly perfect aqueous solution. The binding stoichiometry of receptor **1** with Al^{3+} and F^- was proposed to be 1:1, respectively, based on Job plot, ^1H NMR titration and ESI-mass spectrometry analysis. The detection limits (1.12 μM for Al^{3+} and 7.01 μM for F^-) of **1** for Al^{3+} and F^- were lower than the World Health Organization guidelines (7.41 μM for Al^{3+} and 79 μM for F^-) for drinking water. Chemosensor **1** was also successfully applied to living cells for simultaneous detection and quantification of both Al^{3+} and F^- . Moreover, the sensing mechanisms of **1** toward Al^{3+} and F^- were explained by theoretical calculations.

© 2016 Elsevier Ltd. All rights reserved.

1. Introduction

Natural abundance of aluminum in the biosphere is around 8% of the total mineral components and it is the most abundant metallic element in the Earth's crust [1,2]. Aluminum is generally used in modern life such as the food additives, water purification, pharmaceuticals and the production of light alloy [3–10]. Because of its multiple uses, a tremendous amount of aluminum ions exceeds the human body's excretory capacity, and the excess is deposited in various tissues and cells. Aluminum's toxicity not only hampers plant growth but also damages the human nervous system to induce Alzheimer's disease, Parkinson's disease amyotrophic lateral sclerosis, etc. [11]. Therefore, detection of Al^{3+} is

crucial in controlling its concentration levels in the biosphere and its harmful effect on human health [12–14].

The design and synthesis of fluoride receptors have become of increasing interest because of its important roles in many biological, medical and chemical processes [15–21]. Proper ingestion of fluoride can prevent and cure dental problems and osteoporosis. However, a high intake of fluoride may cause fluorosis, and also lead to nephrotoxic changes and cancer in humans [22–26]. Thus, there are many efforts devoted to the development of fluorescent chemical sensors for fluoride. A variety of fluorescent fluoride sensors based on hydrogen bonding interactions and fluoride ion-induced chemical reactions have been synthesized. However, the number of fluoride probes suitable for cell-imaging applications is still very limited due to the requirements that a chemosensor has to meet for applications in reality. Such requirements include high sensitivity for fluoride in water, a high cell permeability, and low/no toxicity [27–33]. Therefore, it is crucial to develop chemosensors capable of detecting fluoride in cell imaging [34].

Besides, the detection of multiple targets with a single receptor would be more effective and economical than a one-to-one analysis process [35,36]. Various sensing procedures for detecting cations

* Corresponding author. Department of Fine Chemistry, Seoul National University of Science and Technology, Seoul 139-743, Republic of Korea.

** Corresponding author. Department of Fine Chemistry, Seoul National University of Science and Technology, Seoul 139-743, Republic of Korea.

E-mail addresses: idtwar@gmail.com (J.J. Lee), chealkim@seoultech.ac.kr (C. Kim).

and anions have been described, including fluorescent chemosensors, colorimetric chemosensors, and electrochemical methods. Fluorescence sensing methods among them are the most promising due to the simplicity of the assay, convenient procedures, analytes with fast response and high sensitivity [37,38]. For this reason, scientists have devoted huge efforts to design fluorescence probes that monitor multiple targets. On the other hand, only a few chemosensors with the electron-withdrawing or -donating groups have been reported, which showed the interesting sensing properties. Therefore, we planned to synthesize a chemosensor with an electron-donating group (*tert*-butyl).

Herein, we report a new Schiff base chemosensor **1** with the *tert*-butyl moiety as an electron-donating group, which was very water-soluble and exhibited an exclusive sensing property toward Al^{3+} and F^- via fluorescence enhancement in a near-perfect aqueous solution. Moreover, *in vitro* studies with fibroblasts in presence of Al^{3+} and F^- showed for the first time that chemosensor **1** could be successfully applied to living cells for simultaneously quantifying both Al^{3+} and F^- .

2. Experimental section

2.1. General information

All the solvents and reagents (analytical grade and spectroscopic grade) were obtained from Sigma-Aldrich and used as received. The Live/Dead assay (LIVE/DEAD[®] Viability/Cytotoxicity Kit) kit was purchased from Life Technologies Company. ^1H NMR and ^{13}C NMR measurements were performed on a Varian 400 MHz and 100 MHz spectrometer and chemical shifts were recorded in ppm. Electrospray ionization mass spectra (ESI-MS) were collected on a Thermo Finnigan (San Jose, CA, USA) LCQTM Advantage MAX quadrupole ion trap instrument. Elemental analysis for carbon, nitrogen, and hydrogen was carried out by using a Flash EA 1112 elemental analyzer (thermo) in Organic Chemistry Research Center of Sogang University, Korea. UV–vis spectra were recorded at room temperature using a Perkin Elmer model Lambda 25 UV/Vis spectrometer. Fluorescence measurements were performed on a Perkin Elmer model LS45 fluorescence spectrometer.

2.2. Synthesis of **1**

8-Hydroxyjulolidine-9-carboxaldehyde (0.65 g, 3 mmol) was dissolved in 20 mL of ethanol, and 2-amino-4-*tert*-butyl phenol (0.49 g, 3 mmol) was added into the solution. The reaction mixture was stirred for 4 h at room temperature until a brown precipitate appeared. The resulting precipitate was filtered and washed 2 times with diethyl ether. The yield: 0.43 g (40%). ^1H NMR (DMSO- d_6 , 400 MHz) δ : 14.37 (s, 1H), 8.57 (s, 1H), 7.24 (d, 1H), 7.00 (d, 1H), 6.86 (s, 1H), 6.82 (d, 1H), 3.23–3.19 (m, 4H), 2.61 (t, $J = 12$ Hz, 2H), 2.57 (t, $J = 12$ Hz, 2H), 1.88–1.81 (m, 4H), 1.27 (s, 9H). ^{13}C NMR (DMSO- d_6 , 100 MHz): δ 161.94, 157.55, 147.42, 146.89, 142.01, 133.20, 129.71, 122.49, 115.60, 115.13, 112.50, 108.41, 105.53, 49.46, 49.10, 31.43, 26.80, 21.66, 20.68, 20.11 ppm. LRMS (ESI): m/z calcd for $\text{C}_{23}\text{H}_{29}\text{N}_2\text{O}_2 + \text{H}^+$ ($[\text{M} + \text{H}^+]$): 365.223; found, 365.467. Anal. Calcd for $\text{C}_{24}\text{H}_{23}\text{N}_3\text{O}_3$ (365.222): C, 75.79; H, 8.78; N, 7.69; Found: C, 75.54; H, 8.49; N, 7.44%.

2.3. Fluorescence measurements of receptor **1** with Al^{3+}

Receptor **1** (2.2 mg, 0.006 mmol) was dissolved in methanol (2 mL) and 3 μL of the receptor **1** (3 mM) was diluted to 2.997 mL bis-tris buffer (10 mM, pH 7.0) in order to make the final concentration of 3 μM . $\text{Al}(\text{NO}_3)_3 \cdot 9\text{H}_2\text{O}$ (7.5 mg, 0.02 mmol) was dissolved in bis-tris buffer (2 mL). 0.45–4.5 μL of the Al^{3+} solution (10 mM)

was transferred to each receptor solution (3 μM) prepared above. After mixing them for 15 min, fluorescence spectra were obtained at room temperature.

2.4. UV–vis measurements of receptor **1** with Al^{3+}

Receptor **1** (2.2 mg, 0.006 mmol) was dissolved in methanol (2 mL) and 20 μL of the receptor **1** (3 mM) was diluted to 2.980 mL bis-tris buffer to make the final concentration of 20 μM . $\text{Al}(\text{NO}_3)_3 \cdot 9\text{H}_2\text{O}$ (7.5 mg, 0.02 mmol) was dissolved in bis-tris buffer (1 mL). 0.3–8.4 μL of the Al^{3+} solution (20 mM) was transferred to each receptor solution (20 μM) prepared above. After mixing them for 15 min, UV–vis absorption spectra were taken at room temperature.

2.5. Competition with other metal ions

Receptor **1** (2.2 mg, 0.006 mmol) was dissolved in methanol (2 mL) and 3 μL of the receptor **1** (3 mM) was diluted to 2.997 mL bis-tris buffer to make the final concentration of 3 μM . MNO_3 ($\text{M} = \text{Na}, \text{K}, 0.02$ mmol), $\text{M}(\text{NO}_3)_2$ ($\text{M} = \text{Mn}, \text{Co}, \text{Ni}, \text{Cu}, \text{Zn}, \text{Cd}, \text{Hg}, \text{Mg}, \text{Ca}, \text{Pb}, 0.02$ mmol), $\text{M}(\text{ClO}_3)_2$ ($\text{M} = \text{Fe}, 0.02$ mmol) and $\text{M}(\text{NO}_3)_3$ ($\text{M} = \text{Al}, \text{Cr}, 0.02$ mmol) were separately dissolved in bis-tris buffer (2 mL). 4.5 μL of each metal solution (10 mM) was taken and added into 3 mL of each receptor **1** solution (3 μM) prepared above to make 5 equiv. Then, 4.5 μL of the $\text{Al}(\text{NO}_3)_3 \cdot 9\text{H}_2\text{O}$ solution (10 mM) was added into the mixed solution of each metal ion and receptor **1** to make 5 equiv. After mixing them for 15 min, fluorescence spectra were taken at room temperature.

2.6. Job plot measurement of Al^{3+}

Receptor **1** (2.2 mg, 0.006 mmol) and $\text{Al}(\text{NO}_3)_3 \cdot 9\text{H}_2\text{O}$ (7.5 mg, 0.02 mmol) were separately dissolved in methanol (1 mL). 200 μL of the receptor **1** solution (3 mM) was diluted to 14.800 mL of bis-tris buffer to make the concentration of 40 μM . 30 μL of the $\text{Al}(\text{NO}_3)_3 \cdot 9\text{H}_2\text{O}$ solution (20 mM) was diluted to 14.970 mL of bis-tris buffer to make the concentration of 40 μM . 2.7, 2.4, 2.1, 1.8, 1.5, 1.2, 0.9, 0.6 and 0.3 mL of the receptor **1** solution were taken and transferred to vials. 0.3, 0.6, 0.9, 1.2, 1.5, 1.8, 2.1, 2.4 and 2.7 mL of the Al^{3+} solution were added to each receptor **1** solution separately. Each vial had a total volume of 3 mL. After shaking the vials for 15 min, fluorescence spectra were taken at room temperature.

2.7. ^1H NMR titration of Al^{3+}

For ^1H NMR titrations of receptor **1** with Al^{3+} , three NMR tubes of receptor **1** (3.6 mg, 0.01 mmol) dissolved in DMSO- d_6 (700 μL) were prepared and then three different concentrations (0, 0.005, and 0.01) of $\text{Al}(\text{NO}_3)_3 \cdot 9\text{H}_2\text{O}$ dissolved in DMF- d_7 were added to each solution of receptor **1**. After shaking them for 15 min, ^1H NMR spectra were taken at room temperature.

2.8. pH effect of Al^{3+}

A series of buffers with pH values ranging from 2 to 12 were prepared by mixing sodium hydroxide solution and hydrochloric acid in bis-tris buffer. After the solution with a desired pH was achieved, receptor **1** (2.2 mg, 0.006 mmol) was dissolved in methanol (2 mL), and then 3 μL of the receptor **1** (3 mM) was diluted with 2.997 mL buffers to make the final concentration of 3 μM . $\text{Al}(\text{NO}_3)_3 \cdot 9\text{H}_2\text{O}$ (7.5 mg, 0.02 mmol) was dissolved in bis-tris buffer (2 mL). 4.5 μL of the Al^{3+} solution (10 mM) was transferred to each receptor solution (3 μM) prepared above. After mixing them

for 15 min, fluorescence spectra were obtained at room temperature.

2.9. Fluorescence measurements of receptor **1** with F^-

Receptor **1** (2.2 mg, 0.006 mmol) was dissolved in methanol (2 mL) and 20 μ L of the receptor **1** (3 mM) was diluted with 2.980 mL bis-tris buffer to make the final concentration of 20 μ M. Tetraethyl ammonium fluoride (TEAF) hydrate (30.8 mg, 0.2 mmol) was dissolved in bis-tris buffer (2 mL). 0.6–7.2 μ L of the fluoride solution (100 mM) was transferred to receptor solution (20 μ M) prepared above. After mixing them for 15 min, fluorescence spectra were obtained at room temperature.

2.10. UV–vis measurements of receptor **1** with F^-

Receptor **1** (2.2 mg, 0.006 mmol) was dissolved in methanol (2 mL) and 30 μ L of the receptor **1** (3 mM) was diluted with 2.970 mL bis-tris buffer to make the final concentration of 30 μ M. TEAF hydrate (30.8 mg, 0.2 mmol) was dissolved in bis-tris buffer (2 mL). 0.9–17.1 μ L of the fluoride solution (100 mM) was transferred to receptor solution (30 μ M) prepared above. After mixing them for 15 min, UV–vis absorption spectra were taken at room temperature.

2.11. Competition with other anions

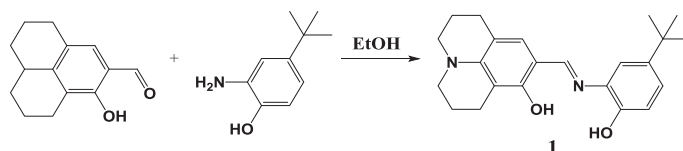
Receptor **1** (2.2 mg, 0.006 mmol) was dissolved in methanol (2 mL) and 20 μ L of receptor **1** (3 mM) was diluted to 2.980 mL bis-tris buffer solution to make the final concentration of 20 μ M. (TEA)X (X = CN^- , OAc^- , F^- , Cl^- , Br^- , I^-), tetrabutylammonium salts ((TBA)X, X = OAc^- , $H_2PO_4^-$, BzO^- , N_3^- , SCN^-) and NaX (X = NO_2^- , SH^-) were separately dissolved in bis-tris buffer (2 mL). 7.2 μ L of each anion solution (100 mM) was taken and added into 3 mL of each receptor **1** solution (10 μ M) prepared above to make 12 equiv. Then, 7.2 μ L of fluoride solution (100 mM) was added into the solution of each anion and receptor **1** to make to 12 equiv. After mixing them for 15 min, fluorescence spectra were taken at room temperature.

2.12. Job plot measurement of receptor **1** with F^-

Receptor **1** (2.2 mg, 0.006 mmol) and TEAF hydrate (30.8 mg, 0.2 mmol) were separately dissolved in methanol (2 mL). 200 μ L of the receptor **1** solution (3 mM) was diluted to 14.800 mL of bis-tris buffer to make the concentration of 40 μ M. 6 μ L of the fluoride solution (100 mM) was diluted to 14.994 mL of bis-tris buffer to make the concentration of 40 μ M. 2.7, 2.4, 2.1, 1.8, 1.5, 1.2, 0.9, 0.6 and 0.3 mL of the receptor **1** solution were taken and transferred to vials. 0.3, 0.6, 0.9, 1.2, 1.5, 1.8, 2.1, 2.4 and 2.7 mL of the fluoride solution were added to each receptor **1** solution separately. Each vial had a total volume of 3 mL. After shaking the vials for 15 min, fluorescence spectra were taken at room temperature.

2.13. NMR titration of receptor **1** with F^-

For 1H NMR titrations of receptor **1** with F^- , five NMR tubes of receptor **1** (3.6 mg, 0.01 mmol) dissolved in $DMSO-d_6$ (700 μ L) were prepared and then five different concentrations (0, 0.005, 0.01, 0.05 and 0.08 mmol) of TEAF dissolved in $DMSO-d_6$ were added to each solution of receptor **1**. After shaking them for 15 min, 1H NMR spectra were taken at room temperature.



Scheme 1. Synthesis of receptor **1**.

2.14. pH effect of F^-

A series of buffers with pH values ranging from 2 to 12 were prepared by mixing sodium hydroxide solution and hydrochloric acid in bis-tris buffer. After the solution with a desired pH was achieved, receptor **1** (2.2 mg, 0.006 mmol) was dissolved in methanol (2 mL), and then 20 μ L of the receptor **1** (20 mM) was diluted with 2.980 mL buffers to make the final concentration of 20 μ M. TEAF hydrate (30.8 mg, 0.2 mmol) was dissolved in bis-tris buffer (2 mL). 7.2 μ L of the fluoride solution (100 mM) was transferred to each receptor solution (20 μ M) prepared above. After mixing them for 15 min, fluorescence spectra were obtained at room temperature.

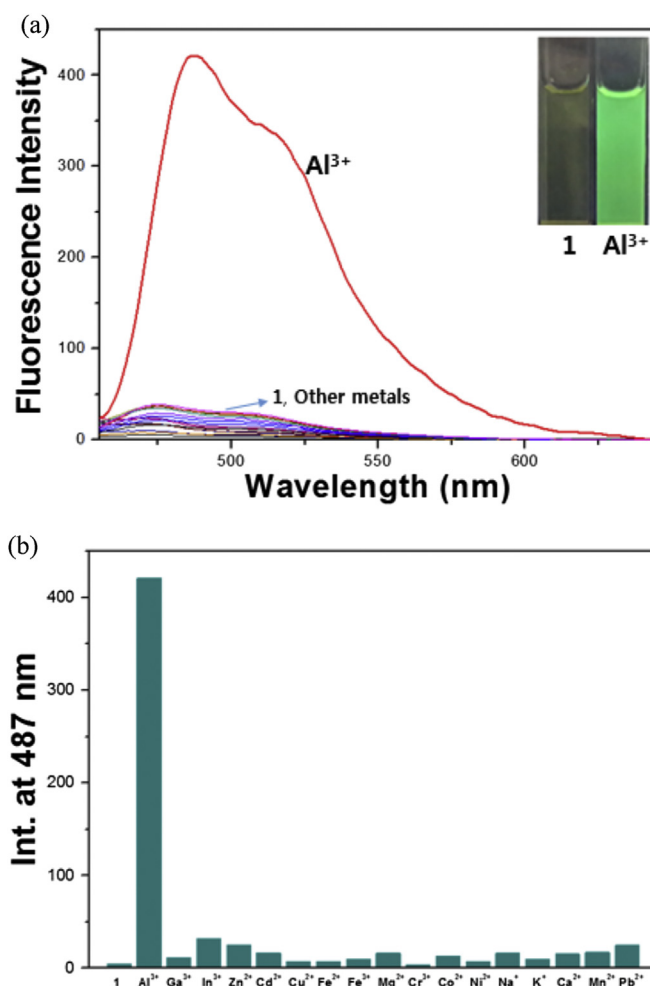


Fig. 1. (a) Fluorescence spectral changes of **1** (3 μ M) in the presence of different metal ions (5 equiv) such as Al^{3+} , Ga^{3+} , In^{3+} , Zn^{2+} , Cd^{2+} , Cu^{2+} , Fe^{2+} , Fe^{3+} , Mg^{2+} , Cr^{3+} , Co^{2+} , Ni^{2+} , Na^+ , K^+ , Ca^{2+} , Mn^{2+} and Pb^{2+} with an excitation of 440 nm in bis-tris buffer solution. (b) Bar graph shows the relative emission intensity of **1** at 487 nm upon treatment with various metal ions.

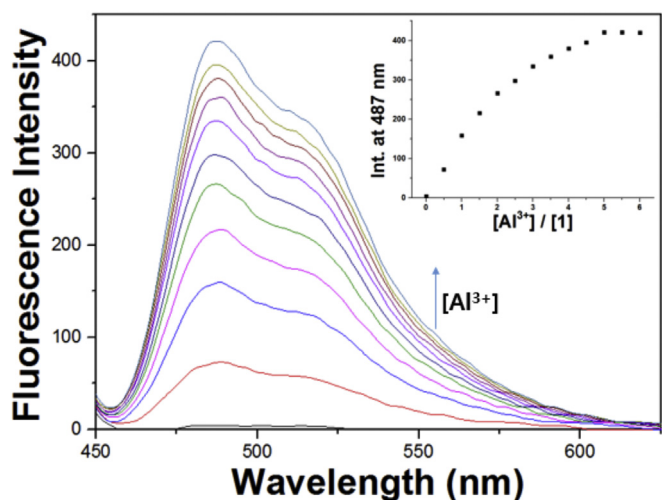


Fig. 2. Fluorescence spectral changes of **1** (3 μM) in the presence of different concentrations of Al^{3+} ions in bis-tris buffer solution. Inset: Fluorescence intensity at 487 nm versus the number of equiv of Al^{3+} added.

2.15. Methods for cell imaging of **1** toward Al^{3+} and F^-

Human dermal fibroblast cells in low passage were cultured in FGM-2 medium (Lonza, Switzerland) supplemented with 10% fetal bovine serum, 1% penicillin/streptomycin in the in vitro incubator with 5% CO_2 at 37 $^\circ\text{C}$. Cells were seeded onto a 10 well plate (SPL Lifesciences, Korea) at a density of 2×10^5 cells per well and then incubated at 37 $^\circ\text{C}$ for 4 h after addition of various concentrations (0–100 μM) of $\text{Al}(\text{NO}_3)_3$ or TEAF dissolved in FGM-2-medium. After washing with phosphate buffered saline (PBS) two times to remove the remaining $\text{Al}(\text{NO}_3)_3$ or TEAF, the cells were incubated with **1** (40 μM) dissolved in FGM-2-medium for 1 h at room temperature. The cells were observed using a microscope

(Olympus, Japan). The fluorescent images of the cells were obtained using a fluorescence microscope (Leica DMLB, Germany) at an excitation wavelength of 425 nm. In order to remove the intracellular levels of Al^{3+} or F^- , the Al^{3+} or F^- -supplemented cells were treated with 100 μM of metal chelator (desferoxamine: DFO).

2.16. Live/dead assay of fibroblast toward **1**, 1-Al^{3+} and 1-F^-

To observe cell viability, a live & dead assay was performed for **1**. Fibroblasts ($P = 5$) were in vitro cultured to reach 70% confluent. The cells were incubated with **1** (40 μM) dissolved in FGM-2-medium for 1 h, 12 h, and 24 h. Reagent (400 μL) of the live & dead assay was added into each cell culture plate. Both viability and morphological changes of the cells were observed by a fluorescence microscope (Leica DMLB, Leica; Wetzlar, Germany). Identical experiments were carried out in the presence of $\text{1-Al}(\text{NO}_3)_3$ (100 μM) and 1-TEAF (100 μM), respectively.

2.17. Theoretical calculations methods of **1** toward Al^{3+} and F^-

All DFT/TDDFT calculations based on the hybrid exchange-correlation functional B3LYP [39,40] were carried out using Gaussian 03 program [41]. The 6-31G** basis set [42,43] was used for all elements (C, O, N, H and Al). In vibrational frequency calculations, there was no imaginary frequency for the optimized geometries of **1**, 1-Al^{3+} and 1-F^- , suggesting that these geometries represented local minima. For all calculations, the solvent effect of water was considered by using the Cossi and Barone's CPCM (conductor-like polarizable continuum model) [44,45]. To investigate the electronic properties of singlet excited states, time-dependent DFT (TDDFT) was performed with the ground state geometries of **1**, 1-Al^{3+} , and 1-F^- . The 25 singlet–singlet excitations were calculated and analyzed. The GaussSum 2.1 [46] was used to calculate the contributions of molecular orbitals in electronic transitions.

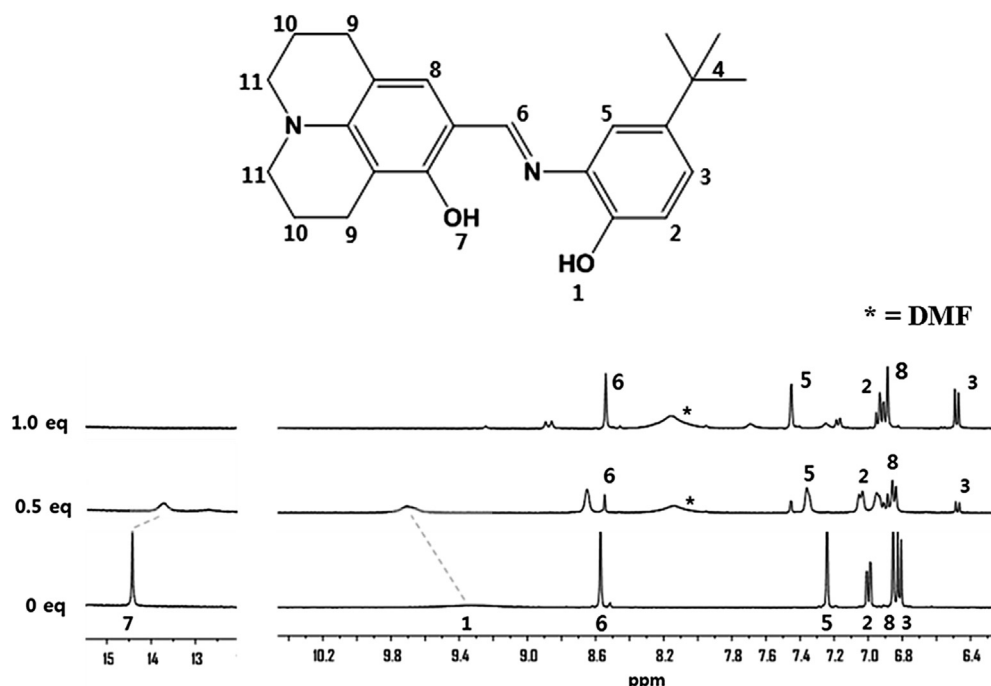
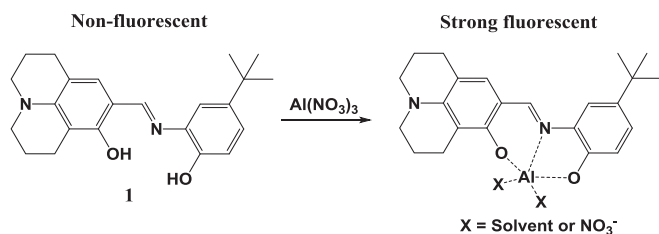


Fig. 3. ^1H NMR titration of **1** with $\text{Al}(\text{NO}_3)_3$.



Scheme 2. Proposed binding mode of receptor **1** with Al^{3+} .

3. Results and discussion

The receptor **1** was obtained by coupling 8-hydroxyjulolidine-9-carboxaldehyde with 2-amino-4-*tert*-butyl phenol with a 40% yield in ethanol (Scheme 1) and characterized by ^1H NMR, ^{13}C NMR, elemental analysis and ESI-MS spectrometry.

3.1. Fluorescence and absorption spectroscopic studies of **1** toward Al^{3+} ion

To examine the fluorescence properties of **1**, the emission was measured with various cations (Al^{3+} , Ga^{3+} , In^{3+} , Zn^{2+} , Cd^{2+} , Cu^{2+} ,

Fe^{2+} , Fe^{3+} , Mg^{2+} , Cr^{3+} , Co^{2+} , Ni^{2+} , Na^+ , K^+ , Ca^{2+} , Mn^{2+} and Pb^{2+}) in bis-tris buffer solution (10 mM, pH 7.0). As shown in Fig. 1, the receptor **1** alone has a very weak fluorescence emission ($\lambda_{\text{ex}} = 440$ nm). When 5 equiv of various metal ions such as Ga^{3+} , In^{3+} , Zn^{2+} , Cd^{2+} , Cu^{2+} , Fe^{2+} , Fe^{3+} , Mg^{2+} , Cr^{3+} , Co^{2+} , Ni^{2+} , Na^+ , K^+ , Ca^{2+} , Mn^{2+} and Pb^{2+} were added to the receptor **1**, it was found that the solution of **1** exhibited no increase of the fluorescence. In contrast, the addition of Al^{3+} resulted in a remarkable enhancement of the emission intensity at 487 nm (90 folds). These results indicated that receptor **1** could be used as a fluorescence chemosensor for Al^{3+} . The selective fluorescence enhancement by Al^{3+} might be due to the effective coordination of Al^{3+} with **1** over other metal ions. This is referred to as chelation-enhanced fluorescence (CHEF) effect: the reaction of a metal ion with a chelating agent induces rigidity in the resulting molecule and tends to produce fluorescence. Also, receptor **1** is poorly fluorescent in part due to excited-state intramolecular proton transfer (ESIPT) [23] involving the phenolic protons. Upon stable chelation with aluminum ion, the C=N isomerization and ESIPT might be inhibited, leading to fluorescence enhancement.

To further investigate the chemosensing properties of **1** toward Al^{3+} , fluorescence titration of the receptor **1** with Al^{3+} ion was

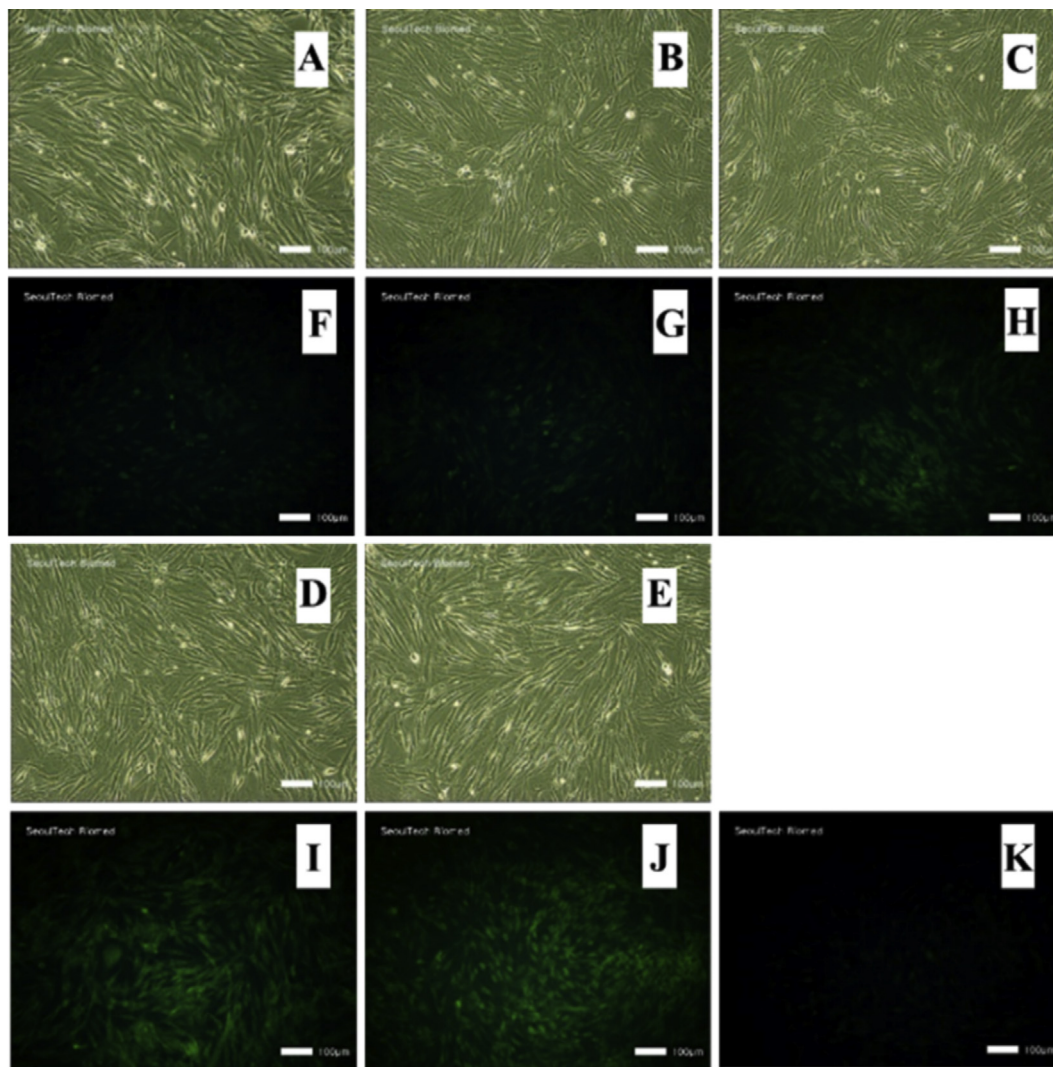


Fig. 4. Fluorescence images of fibroblasts cultured with Al^{3+} and **1**. Cells were exposed to 0 (A and F), 15 (B and G), 50 (C and H), 80 (D and I), 100 (E, J and K) μM $\text{Al}(\text{NO}_3)_3 \cdot 9\text{H}_2\text{O}$ for 4 h and then later with **1** (40 μM) for 30 min. Fluorescence image of K was taken 30 min after J was treated with DFO (100 μM). The top images (A–E) were observed with the light microscope and the bottom images (F–K) were taken with a fluorescence microscope. The scale bar was 100 μm .

performed (Fig. 2) The emission intensity of **1** at 487 nm steadily increased until the amount of Al^{3+} reached 5 equiv. The photophysical properties of **1** were examined using UV–vis spectrometry (Fig. S1). Upon the addition of Al^{3+} to a solution of **1**, the absorption band at 440 nm decreased and was saturated with 2.8 equiv of Al^{3+} with an isosbestic point at 291 nm, indicating a clean conversion of **1** into the 1-Al^{3+} complex.

The binding mode between **1** and Al^{3+} was determined by using Job plot [47] analysis (Fig. S2), which exhibited 1:1 complexation stoichiometry. The formation of 1-Al^{3+} complex was also further confirmed by ESI-MS spectrometry analysis. The positive ion mass spectrum indicated that the peak at m/z 544.867 was assigned to $[\text{1}+\text{Al}^{3+}-2\text{H}+4\text{ solvents}]^+$ (Fig. S3).

The interaction between receptor **1** and Al^{3+} was further studied through ^1H NMR titration (Fig. 3). Upon addition of **1** equiv of Al^{3+} , the protons of the two hydroxyl groups at 9.33 and 14.42 ppm disappeared due to deprotonation. The H_6 of the $\text{C}=\text{N}$ moiety, H_3 and H_2 shifted upfield by 0.02, 1.70 and 0.07 ppm, respectively, while the aromatic protons H_5 and H_8 shifted downfield. There was no shift in the position of proton signals on further addition of Al^{3+} (>1 equiv), which indicates a 1:1 binding of **1** to Al^{3+} . Based on the Job plot, ESI-mass spectrometry analysis, and ^1H NMR titration, we proposed the structure of a 1:1 complex of **1** and Al^{3+} , as shown in Scheme 2.

From the results of fluorescence titration, the association constant of the 1-Al^{3+} complex was determined as $2.1 \times 10^5 \text{ M}^{-1}$ on the basis of Benesi–Hildebrand equation (Fig. S4). This value is within the range of those ($10^3 \sim 10^9$) reported for Al^{3+} -chemosensors [48–62]. For practical application, the detection limit was also an important parameter. Thus, the detection limit ($3\sigma/k$) of receptor **1** for the analysis of Al^{3+} ion was calculated and found to be $1.12 \mu\text{M}$ (Fig. S5) [63]. The detection limit of **1** for Al^{3+} was lower than the value ($7.41 \mu\text{M}$) recommend by WHO in drinking water [64].

To check the practical applicability of **1** as a selective fluorescence sensor for Al^{3+} , the competition experiments were conducted in the presence of Al^{3+} mixed with other metal ions, such as Ga^{3+} , In^{3+} , Zn^{2+} , Cd^{2+} , Cu^{2+} , Fe^{2+} , Fe^{3+} , Mg^{2+} , Cr^{3+} , Co^{2+} , Ni^{2+} , Na^+ , K^+ , Ca^{2+} , Mn^{2+} , and Pb^{2+} . When **1** was treated with 5 equiv of Al^{3+} in the presence of the same concentration of other metal ions (Fig. S6), there was no or small interferences for most interfering metal ions except for Cu^{2+} , Fe^{2+} , Fe^{3+} and Cr^{3+} , which completely interfered.

For biological applications, the pH dependence of the 1-Al^{3+} complex was examined. Over the pH range tested, the fluorescence intensity of 1-Al^{3+} displayed a strong pH dependence (Fig. S7). An intense and stable fluorescence of 1-Al^{3+} found in the pH range of 5.0–7.5 warrants its application under physiological conditions, without any change in detection results.

To further demonstrate the practical biological application of **1**, fluorescence imaging experiments were carried out in living cells (Fig. 4). Adult human dermal fibroblasts were first incubated with various concentrations of Al^{3+} (0, 15, 50, 80 and $100 \mu\text{M}$) for 4 h and then exposed to **1** ($40 \mu\text{M}$) for 30 min before imaging. The fibroblast cells with neither Al^{3+} nor **1** did not exhibit fluorescence. However, the intensity of fluorescence within the cell increased as the Al^{3+} concentration increased from 15 to $100 \mu\text{M}$. The mean intensities of the fluorescent region were evaluated by Icy software (Fig. S8). The detection limit was found to be $11.9 \mu\text{M}$. When the Al^{3+} -supplemented cells (Fig. 4j) were treated with $100 \mu\text{M}$ of metal chelator (Desferoxamine; DFO), the fluorescent intensity disappeared, indicating that observed intracellular fluorescence enhancements were due to the changing levels in the Al^{3+} -supplemented cells. Moreover, the biocompatibility of **1** and 1-Al^{3+} complex was also examined with the living cells (Figs. S9 and S10). All the fibroblasts were alive for 12 h, while a few cells were dead after 24 h. These

results demonstrated that a new sensor **1** could be a suitable and biocompatible sensor for detecting Al^{3+} in living cells.

3.2. Fluorescence and absorption spectroscopic studies of **1** toward fluoride

To examine the fluorescent properties of **1** toward various anions, the emission was also investigated with various anions (F^- , CN^- , OAc^- , Cl^- , Br^- , I^- , H_2PO_4^- , BzO^- , N_3^- , SCN^- , NO_2^- and SH^-) in bis-tris buffer solution (10 mM, pH 7.0). Receptor **1** alone has a weak fluorescence emission (Fig. 5). Upon the addition of 12 equiv of each anion, only F^- resulted in a drastic enhancement (83 folds) of the emission intensity at 495 nm ($\lambda_{\text{ex}} = 440 \text{ nm}$), while other anions showed either no or slight increase in the fluorescence spectra relative to the free receptor **1**.

To further investigate the chemosensing properties of **1**, the fluorescence titration of the receptor **1** with F^- was investigated. The emission intensity of **1** at 495 nm gradually increased until the amount of F^- reached 12 equiv (Fig. 6). The photophysical properties of **1** were also examined using UV–vis spectrometry. The absorption band at 450 nm decreased and a new absorbance intensity at 525 nm increased with an isosbestic point at 490 nm (Fig. S11), suggesting that the only product was produced from **1** binding to F^- .

The Job plot [47] showed a 1:1 stoichiometry between **1** and F^- (Fig. S12). To further examine the binding mode between **1** and F^- ,

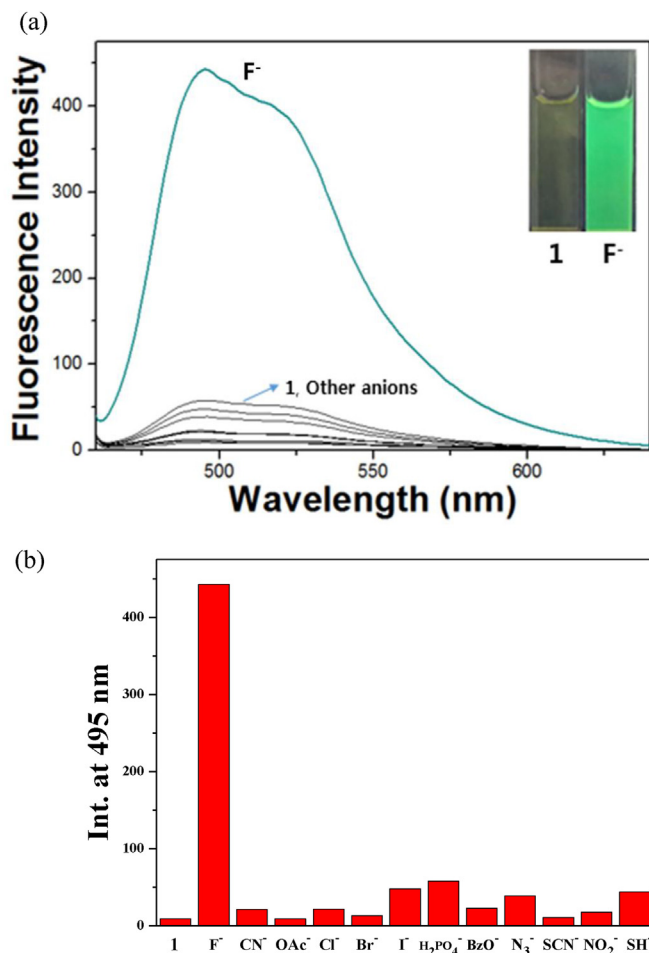


Fig. 5. (a) Fluorescence spectral changes of **1** ($20 \mu\text{M}$) in the presence of different anions (12 equiv) such as F^- , CN^- , OAc^- , Cl^- , Br^- , I^- , H_2PO_4^- , BzO^- , N_3^- , SCN^- , NO_2^- and SH^- with an excitation of 440 nm in bis-tris buffer solution. (b) Bar graph shows the relative emission intensity of **1** at 495 nm upon treatment with various anions.

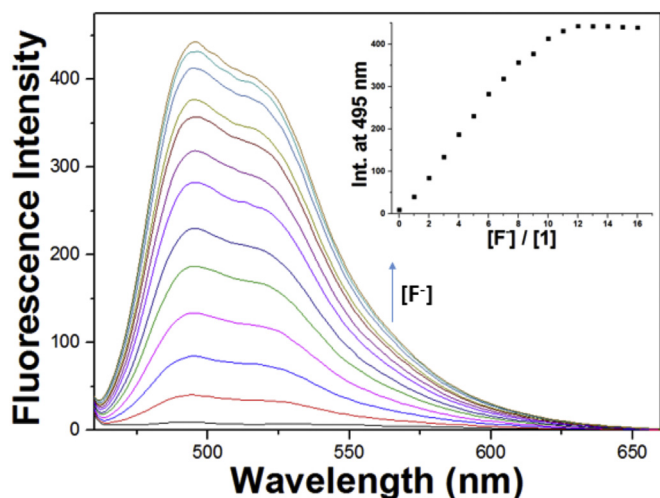


Fig. 6. Fluorescence spectral changes of **1** (20 μM) in the presence of different concentrations of F^- in bis-tris buffer solution. Inset: Fluorescence intensity at 495 nm versus the number of equiv of F^- added.

ESI-mass experiment was carried out (Fig. S13). A peak at m/z 727.000 was assigned to $[\mathbf{1} + \text{F}^- - \text{H} + 2\text{TEA} + \text{Cl}^- + 2 \text{ solvents}]$.

The ^1H NMR investigation was performed to further understand the nature of interaction between sensor **1** and fluoride (Fig. 7).

Upon addition of 1 equiv of TEAF as a fluoride source, the proton signals of two OH moieties at 9.30 and 14.36 ppm gradually disappeared. The proton signal of H_6 showed a downfield-shift, while most of aromatic protons were shifted upfield. On excess addition of F^- (8 equiv) to **1** solution, a new peak at 15.5 ppm appeared, indicating the formation of $[\text{HF}_2]^-$ species. Based on ^1H NMR titrations and ESI-mass spectrometry analysis, we proposed the sensing mechanism of **1** for F^- as shown in Scheme 3.

Based on the fluorescence titration data, the association constant for **1** with F^- was determined as $1.4 \times 10^4 \text{ M}^{-1}$ from Benesi–Hildebrand equations (Fig. S14). This value is slightly greater than those ($10^2 \sim 10^4$) reported for F^- -chemosensors [65–71]. The detection limit of receptor **1** as a fluorescence sensor for the analysis of F^- was found to be 7.01 μM (Fig. S15) [63]. This value is far below the WHO guideline (79 μM) for drinking water [72].

To explore the ability of **1** as a fluorescence chemosensor for fluoride, the competition experiments were conducted in the presence of F^- mixed with various competing anions (Fig. 8). When receptor **1** was treated with 12 equiv of F^- in the presence of the same concentration of other anions, other background anions had small or no obvious interference with detection of F^- ion, except for 82% and 53% interferences of NO_2^- and SH^- . Thus, **1** could be used as a selective fluorescence sensor for F^- in the presence of other competing anions.

For biological applications, the pH sensitivity of F^- detection by **1** was examined by fluorescence measurements (Fig. S16). While

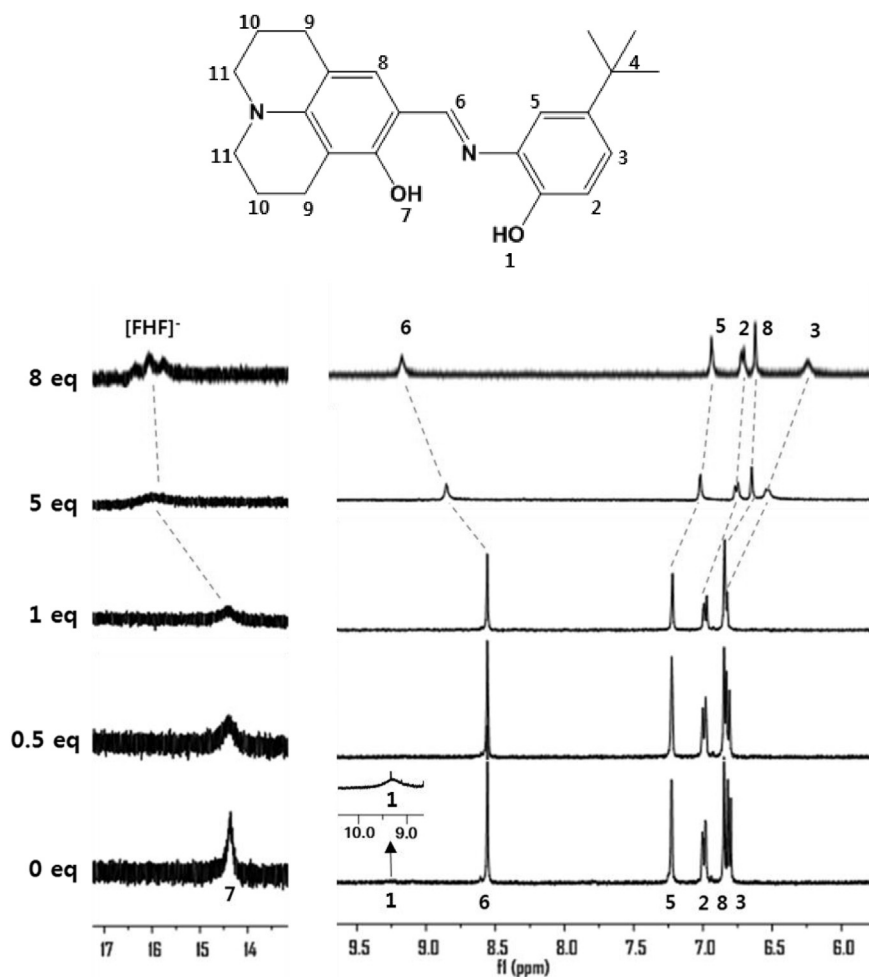
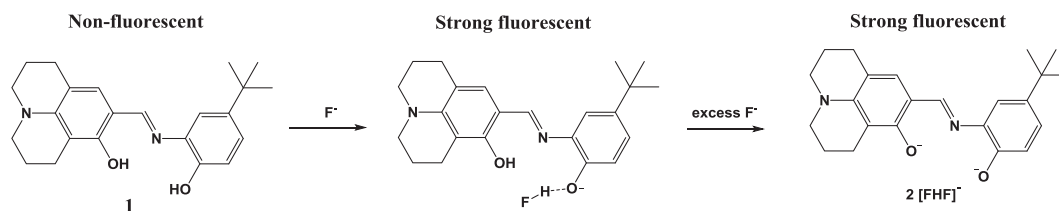


Fig. 7. ^1H NMR titration of **1** with TEAF.



Scheme 3. Proposed sensing mechanism of F^- by **1**.

the fluorescence of **1-F⁻** was very weak at low (2–4) and high pH (10–12), its intense and stable fluorescence was observed in the pH range of 5–10, which permits its application under physiological conditions, without any change in detection results.

To further know the potential of **1** to detect F^- in living matrices, fluorescence imaging experiments were carried out in living cells (Fig. 9). Adult human dermal fibroblasts were incubated with various concentrations of F^- (0, 15, 50, 80 and 100 μM) for 4 h and then exposed to **1** (40 μM) for 1 h before imaging. The intensity and region of the fluorescence within the cell with **1** increased as the F^- concentration increased from 15 to 100 μM . The mean intensities of the fluorescent region were also evaluated by Icy software [73] and the detection limit was found to be 18.1 μM (Fig. S17). The biocompatibility of **1-F⁻** was also examined with the living cells (Fig. S18). All the fibroblasts were still alive until 12 h, while some cells were dead after 24 h. These results demonstrated that a new sensor **1** could be a suitable and biocompatible sensor for detecting F^- in living cells.

On the other hand, whether Al^{3+} distinguishes from F^- in fluorescent cell applications must be considered, because both **1- Al^{3+}** and **1-F⁻** showed the same fluorescence in the living cells. Thus, we treated both **1- Al^{3+}** and **1-F⁻**-supplemented cells with the metal chelator DFO (Figs. 4K and 9K). The original fluorescence of the **1-F⁻**-supplemented cells was retained for 4 h (Fig. 9J), while the **1- Al^{3+}** -supplemented cells lost the fluorescence within 30 min after DFO was added (Fig. 4K). These results demonstrated that Al^{3+} could be distinguished from F^- in fluorescent cell applications, and that the fluorescence of **1- Al^{3+}** in cells was Al^{3+} -based. Moreover, in vitro studies with fibroblasts in presence of Al^{3+} and F^- showed for the first time that chemosensor **1** could be successfully applied to living cells for simultaneous quantification of both Al^{3+} and F^- .

3.3. Theoretical sensing mechanism of **1** toward Al^{3+} and F^-

To further understand the sensing mechanism, theoretical calculations were performed for **1**, **1- Al^{3+}** complex and **1-F⁻**. The energy-minimized structures of chemosensor **1** and **1- Al^{3+}** complex were obtained from various possible isomers at DFT/B3LYP/6-31G** level. Their energy-minimized structures along with bond lengths and angles were shown in Fig. S19. The structures of **1** and **1- Al^{3+}** complex had planar conformations. In case of **1-F⁻**, the deprotonation of the (*tert*-butyl)phenol by F^- was observed, which produced a strong hydrogen bond with the bond length of 1.0368 Å between 6H and 7F. As the excitations of fluorescence for **1**, **1- Al^{3+}** complex and **1-F⁻** were relevant to their absorptions, time-dependent density functional theory (TD-DFT) calculations were also performed. In the case of **1**, the main molecular orbital (MO) contribution of the first lowest excited state was determined for HOMO \rightarrow LUMO transition (439.41 nm, Fig. S20), which was $\pi \rightarrow \pi^*$ transition. For **1- Al^{3+}** complex (Fig. S21), the second lowest excited state with oscillator strength of 1.0914 was considered as a major excitation, which was also determined for HOMO \rightarrow LUMO transition (430.87 nm, Fig. S21b). There were no obvious changes in

the electronic transitions between **1** and **1- Al^{3+}** complex. These results suggested that the sensing mechanism of **1** toward Al^{3+} originated from the rigid structure of **1- Al^{3+}** complex, which might inhibit the non-radioactive process such as C=N isomerization and ESIPT process [38,74]. For **1-F⁻**, the main molecular orbital (MO) contribution of the first lowest excited state was determined for HOMO \rightarrow LUMO transition (439.03 nm, Fig. S22), which is similar to the transition between **1** and **1- Al^{3+}** . These results led us to propose that the strong hydrogen bond between **1** and F^- induced the inhibition of the non-radioactive process, resulting in the fluorescence enhancement.

4. Conclusion

We have synthesized a bifunctional fluorescence sensor **1** based on the combination of 2-amino-4-*tert*-butyl phenol and 8-hydroxyjulolidine-9-carboxaldehyde. The sensor **1** with the electron-donating group (*tert*-butyl) was very water-soluble and showed selective response to both Al^{3+} and F^- with turn-on fluorescence enhancement in near-perfect aqueous solution. The detection limits of **1** for Al^{3+} and F^- were lower than WHO guidelines for drinking water. Chemosensor **1** could be successfully applied to living cells for simultaneous detection and quantification of both Al^{3+} and F^- . Additionally, the sensing mechanisms of **1** toward Al^{3+} and F^- were explained by theoretical calculations. These results provide a useful sensing strategy for the concept of 'a single chemosensor for multiple analytes' in both environment and in vitro systems.

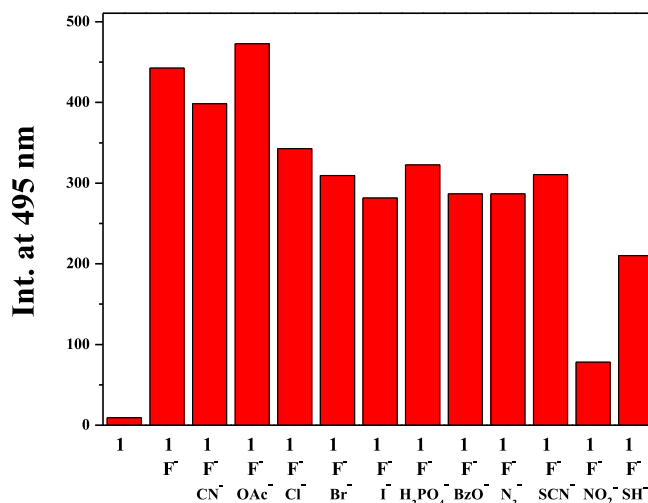


Fig. 8. Competitive selectivity of **1** (20 μM) toward F^- (12 equiv) in the presence of other anions (12 equiv) in bis-tris buffer solution.

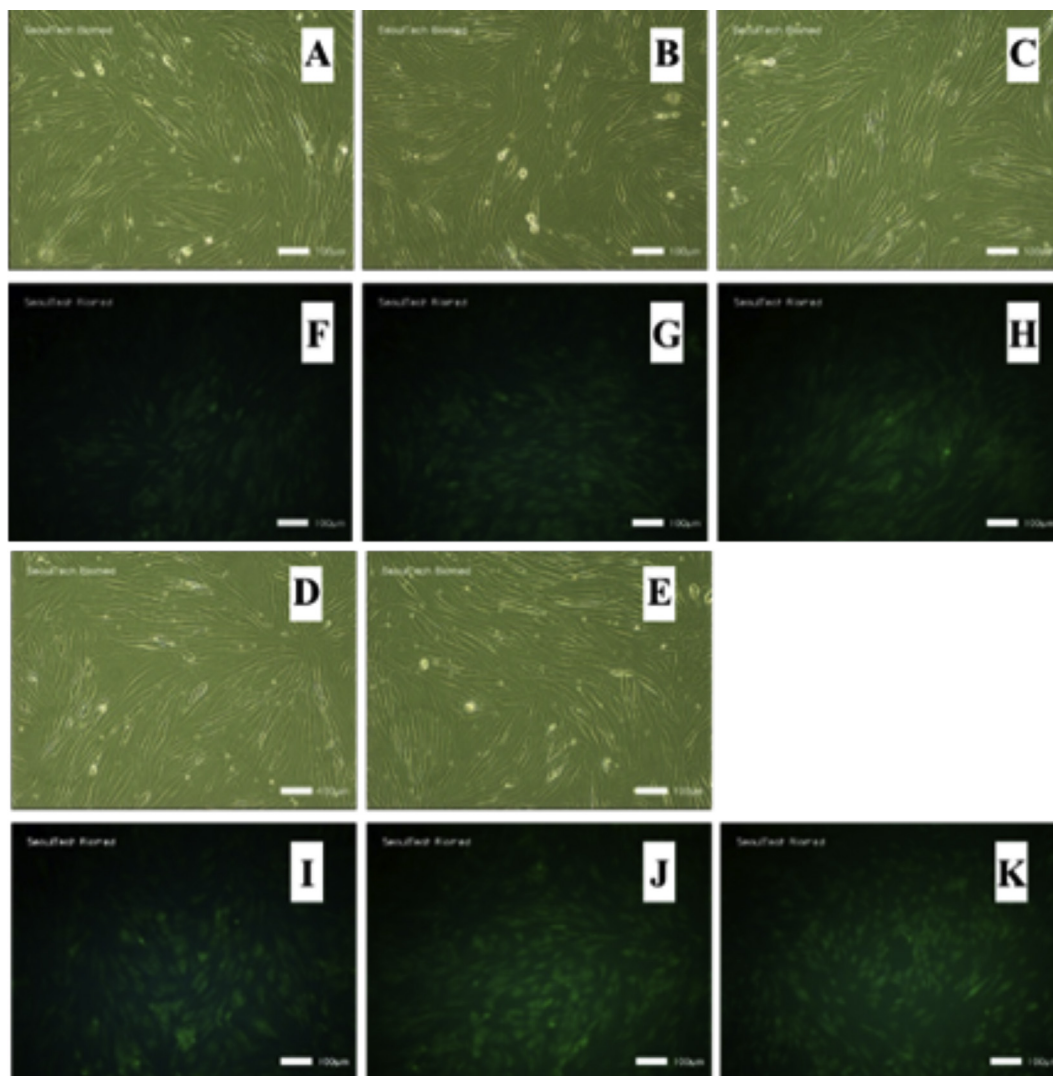


Fig. 9. (a) Fluorescence images of fibroblasts cultured with F^{-} and **1**. Cells were exposed to 0 (A and F), 15 (B and G), 50 (C and H), 80 (D and I), 100 (E, J and K) μM TEAF for 4 h and then later with **1** (40 μM) for 30 min. Fluorescence image of K was taken 30 min after J was treated with DFO (100 μM). The top images (A–E) were observed with the light microscope and the bottom images (F–K) were taken with a fluorescence microscope. The scale bar was 100 μm .

Acknowledgments

Financial support from Basic Science Research Program through the National Research Foundation of Korea (NRF) funded by the Ministry of Education, Science and Technology (NRF-2014R1A2A1A11051794) are gratefully acknowledged.

Appendix A. Supplementary data

Supplementary data related to this article can be found at <http://dx.doi.org/10.1016/j.dyepig.2016.02.016>.

References

- [1] Sahana A, Benerjee A, Lohar S, Banik A, Mukhopadhyay SK, Safin DA, et al. FRET based tri-color emissive rhodamine-pyrene conjugate as an Al^{3+} selective colorimetric and fluorescence sensor for living cell imaging. *Dalton Trans* 2013;42:13311–4.
- [2] Das S, Dutta M, Das D. Fluorescent probes for selective determination of trace level Al^{3+} : recent developments and future prospects. *Anal Methods* 2013;5: 6262–85.
- [3] Barceló J, Poschenrieder C. Fast root growth responses, root exudates, and internal detoxification as clues to the mechanisms of aluminum toxicity and resistance: a review. *Environ Exp Bot* 2002;48:75–92.
- [4] Wang D, Ke Y, Guo H, Chen J, Weng W. A novel highly selective colorimetric sensor for aluminum (III) ion using Schiff base derivative. *Spectrochim Acta Part A* 2014;122:268–72.
- [5] Jang YJ, Yeon YH, Yang HY, Noh JY, Hwang IH, Kim C. A colorimetric and fluorescent chemosensor for selective detection of Cr^{3+} and Al^{3+} . *Inorg Chem Commun* 2013;33:48–51.
- [6] Kim KB, You DM, Jeon JH, Yeon YH, Kim JH, Kim C. A fluorescent and colorimetric chemosensor for selective detection of aluminum in aqueous solution. *Tetrahedron Lett* 2014;55:1347–52.
- [7] Das S, Dutta M, Das D. Fluorescent probes for selective determination of trace level Al^{3+} : recent developments and future prospects. *Anal Methods* 2013;5: 6262–85.
- [8] Jung HS, Kwon PS, Lee JW, Kim JI, Hong CS, Kim JW, et al. Coumarin-derived Cu^{2+} -selective fluorescence sensor: synthesis, mechanisms, and applications in living cells. *J Am Chem Soc* 2009;131:2008–12.
- [9] You J, Hu H, Zhou J, Zhang L, Zhang Y, Kondo T. Novel cellulose polyampholyte-gold nanoparticle-based colorimetric competition assay for the detection of cysteine and mercury(II). *Langmuir* 2013;29: 5085–92.
- [10] Li Z, Hu Q, Li C, Dou J, Cao J, Chen W, et al. A 'turn-on' fluorescent chemosensor based on rhodamine-N-(3-aminopropyl)-imidazole for detection of Al^{3+} ions. *Tetrahedron Lett* 2014;55:1258–62.
- [11] Fasman GD. Aluminum and Alzheimer's disease: model studies. *Coord Chem Rev* 1996;149:125–65.

- [12] Nayak P. Aluminum: impacts and disease. *Environ Res* 2002;89:101–15.
- [13] de Silva AP, Gunaratne HQN, Gunlaugsson T, Huxley AJM, McCoy CP, Rademacher JT, et al. Signaling recognition events with fluorescent sensors and switches. *Chem Rev* 1997;97:1515–66.
- [14] Valeur B, Leray I. Design principles of fluorescent molecular sensors for cation recognition. *Coord Chem Rev* 2000;205:3–40.
- [15] Zhang G, Wang L, Cai X, Zhang L, Yu J, Wang A. A new diketopyrrolopyrrole (DPP) derivative bearing boronate group as fluorescent probe for fluoride ion. *Dyes Pigments* 2013;98:232–7.
- [16] Kim Y-J, Kwak H, Lee SJ, Lee JS, Kwon HJ, Nam SH, et al. Urea/thiourea-based colorimetric chemosensors for the biologically important ions: efficient and simple sensors. *Tetrahedron* 2006;62:9635–40.
- [17] Kang J, Lee YJ, Lee SK, Lee JH, Park JJ, Kim Y, et al. A naked-eye detection of fluoride with urea/thiourea receptors which have both a ben-zophenone group and a nitrophenyl group as a signalling group. *Supramol Chem* 2010;22:267–73.
- [18] Kang J, Jang SP, Kim YH, Lee JH, Park EB, Lee HG, et al. Novel receptors with quinoline and amide moieties for the biologically important ions. *Tetrahedron Lett* 2010;51:6658–62.
- [19] Kang J, Lee JH, Kim YH, Lee SK, Kim EY, Lee HG, et al. Simpleurea/thiourea sensors for the biologically important ions. *J Incl Phenom Macrocycl Chem* 2011;70:29–35.
- [20] Park JJ, Kim Y-H, Kim C, Kang J. Fine tuning of receptor polarity for the development of selective naked eye anion receptor. *Tetrahedron Lett* 2011;52:3361–6.
- [21] Matsui H, Morimoto M, Horimoto K, Nishimura Y. Some characteristics of fluoride-induced cell death in rat thymocytes: cytotoxicity of sodium fluoride. *Toxicol Vitro* 2007;21:1113–20.
- [22] Horowitz HS. The 2001 CDC recommendations for using fluoride to prevent and control dental caries in the United States. *J Public Health Dent* 2003;63:3–8.
- [23] Ayoob S, Gupta AK. Fluoride in drinking water: a review on the status and stress effects. *Crit Rev Environ Sci Technol* 2006;36:433–87.
- [24] Xu Z, Kim SK, Han SJ, Lee C, Kociok-Kohn G, James TD, et al. Ratiometric fluorescence sensing of fluoride ions by an asymmetric bidentate receptor containing a boronic acid and imidazolium group. *Eur J Org Chem* 2009;18:3058–65.
- [25] Xu WJ, Liu SJ, Zhao XY, Sun S, Cheng S, Ma TC, et al. Cationic Iridium(III) complex containing both triarylboron and carbazole moieties as a ratiometric fluoride probe that utilizes a switchable triplet-singlet emission. *Chem Eur J* 2010;16:7125–33.
- [26] Zhao CH, Sakuda E, Wakamiya A, Yamaguchi S. Highly emissive diborylphenylene-containing Bis(phenylethynyl)benzenes: structure-photophysical property correlations and fluoride ion sensing. *Chem Eur J* 2009;15:10603–12.
- [27] Mallick A, Roy UK, Haldar B, Pratihari S. A newly developed highly selective ratiometric fluoride ion sensor: spectroscopic, NMR and density functional studies. *Analyst* 2012;137:1247–51.
- [28] Im HG, Kim HY, Choi MG, Chang SK. Reaction-based dual signaling of fluoride ions by resorufin sulfonates. *Org Biomol Chem* 2013;11:2966–71.
- [29] Sarka SK, Thilagar P. A borane-bithiophene-BODIPY triad: intriguing tricolor emission and selective fluorescence response towards fluoride ions. *Chem Commun* 2013;49:8558–60.
- [30] Li HY, Lalancette RA, Jäkle F. Turn-on fluorescence response upon anion binding to dimesitylboryl-functionalized quaterthiophene. *Chem Commun* 2011;47:9378–80.
- [31] Tomat E, Lippard SJ. Ratiometric and intensity-based zinc sensors built on rhodol and rhodamine platforms. *Inorg Chem* 2010;49:9113–5.
- [32] Zyryanov GV, Palacios MA, Anzenbacher Jr P. Rational design of a fluorescence-turn-on sensor array for phosphates in blood serum. *Angew Chem Int Ed* 2007;46:7849–52.
- [33] Xue L, Li GP, Zhu DJ, Liu Q, Jiang H. Rational design of a ratiometric and targetable fluorescent probe for imaging lysosomal zinc ions. *Inorg Chem* 2012;51:10842–9.
- [34] Ghosh K, Kar D, Fröhlich R, Chattopadhyay AP, Samadder A, Khuda-Bukhsh AR. O-tert-Butyldiphenylsilyl coumarin and dicoumarol: a case toward selective sensing of F⁻ ions in organic and aqueous environments. *Analyst* 2013;138:3038–45.
- [35] Beer PD, Gale PA. Anion recognition and sensing: the state of the art and future perspectives. *Angew Chem Int Ed Engl* 2001;40:486–516.
- [36] Sahoo SK, Sharma D, Bera RK, Crisponi G, Callan JF. Iron (III) selective molecular and supramolecular fluorescent probes. *Chem Soc Rev* 2012;41:7195–227.
- [37] Das S, Karak D, Lohar S, Banerjee A, Sahana A, Das D. Interaction of a naphthalene based fluorescent probe with Al³⁺: experimental and computational studies. *Anal Methods* 2012;4:3620–4.
- [38] Lee JJ, Park GJ, Kim YS, Lee SY, Kim C. A water-soluble carboxylic-functionalized chemosensor for detecting Al³⁺ in aqueous media and living cells: experimental and theoretical studies. *Biosens Bioelectron* 2015;69:226–9.
- [39] Becke AD. Density-functional thermochemistry. III. The role of exact exchange. *J Chem Phys* 1993;98:5648–52.
- [40] Lee C, Yang W, Parr RG. Development of the Colle-Salvetti correlation-energy formula into a functional of the electron density. *Phys Rev B* 1988;37:785–9.
- [41] Frisch MJ, Trucks GW, Schlegel HB, Scuseria GE, Robb MA, Cheeseman JR, et al. Gaussian 03, revision D.01. Wallingford CT: Gaussian, Inc; 2004.
- [42] Hariharan PC, Pople JA. The influence of polarization functions on molecular orbital hydrogenation energies. *Theor Chim Acta* 1973;28:213–22.
- [43] Francl MM, Pietro WJ, Hehre WJ, Binkley JS, Gordon MS, DeFrees DF, et al. Self-consistent molecular orbital methods. XXIII. A polarization-type basis set for second-row elements. *J Chem Phys* 1982;77:3654–65.
- [44] Barone V, Cossi M. Quantum calculation of molecular energies and energy gradients in solution by a conductor solvent model. *J Phys Chem A* 1998;102:1995–2001.
- [45] Cossi M, Barone V. Time-dependent density functional theory for molecules in liquid solutions. *J Chem Phys* 2001;115:4708–17.
- [46] O'Boyle NM, Tenderholt AL. cclib: a library for package-independent computational chemistry algorithms. *J Comput Chem* 2008;29:839–45.
- [47] Job P. Formation and stability of inorganic complexes in solution. *Ann Chim* 1928;9:113–203.
- [48] Kim S, Noh JY, Kim KY, Kim JH, Kang HK, Nam S-W, et al. Salicylimine-based fluorescent chemosensor for aluminum ions and application to bioimaging. *Inorg Chem* 2012;51:3597–602.
- [49] Wang L, Li H, Cao D. A new photoresponsive coumarin-derived Schiff base: chemosensor selectively for Al³⁺ and Fe³⁺ and fluorescence “turn-on” under room light. *Sens Actuators B* 2013;181:749–55.
- [50] Karak D, Lohar S, Sahana A, Guha S, Banerjee A, Das D. An Al³⁺ induced green luminescent fluorescent probe for cell imaging and naked eye detection. *Anal Methods* 2012;4:1906–8.
- [51] Karak D, Lohar S, Banerjee A, Sahana A, Hauli I, Mukhopadhyay SK, et al. Interaction of soft donor sites with a hard metal ion: crystallographically characterized blue emitting fluorescent probe for Al(III) with cell staining studies. *RSC Adv* 2012;2:12447–54.
- [52] Chen Y, Mi Y, Xiang QXJ, Fan H, Luo X, Xia S. A new off-on chemosensor for Al³⁺ and Cu²⁺ in two different systems based on a rhodamine B derivative. *Anal Methods* 2013;5:4818–23.
- [53] Chereddy NR, Nagaraju P, Raju MVN, Krishnaswamy VR, Korrapati PS, Bangal PR, et al. A novel FRET ‘off-on’ fluorescent probe for the selective detection of Fe³⁺, Al³⁺ and Cr³⁺ ions: Its ultrafast energy transfer kinetics and application in live cell imaging. *Biosens Bioelectron* 2015;68:749–56.
- [54] Gui S, Huang Y, Hu F, Jin Y, Zhang G, Yan L, et al. Fluorescence turn-on chemosensor for highly selective and sensitive detection and bioimaging of Al³⁺ in living cells based on ion-induced aggregation. *Anal Chem* 2015;87:1470–4.
- [55] Cao W, Zheng X-J, Sun J-P, Wong W-T, Fang D-C, Zhang J-X, et al. A highly selective chemosensor for Al(III) and Zn(II) and its coordination with metal ions. *Inorg Chem* 2014;53:3012–21.
- [56] Peng L, Zhou Z, Wang X, Wei R, Li K, Xiang Y, et al. A ratiometric fluorescent chemosensor for Al³⁺ in aqueous solution based on aggregation-induced emission and its application in live-cell imaging. *Anal Chim Acta* 2014;829:54–9.
- [57] Shooraa SK, Jaina AK, Gupta VK. A simple Schiff base based novel optical probe for aluminium (III) ions. *Sens Actuators B* 2015;216:86–104.
- [58] Kim H, Rao BA, Jeong JW, Mallick S, Kang S-M, Choi JS, et al. A highly selective dual-channel Cu²⁺ and Al³⁺ chemodosimeter in aqueous systems: sensing in living cells and microfluidic flows. *Sens Actuators B* 2015;210:173–82.
- [59] Alici O, Erdemir S. A cyanobiphenyl containing fluorescence “turn on” sensor for Al³⁺ ion in CH₃CN–water. *Sens Actuators B* 2015;208:159–63.
- [60] Liang C, Bu W, Li C, Men G, Deng M, Jiangyao Y, et al. A highly selective fluorescent sensor for Al³⁺ and the use of the resulting complex as a secondary sensor for PPI in aqueous media: its applicability in live cell imaging. *Dalton Trans* 2015;44:11352–9.
- [61] Goswami S, Manna A, Paul S, Maity AK, Saha P, Quah CK, et al. FRET based ‘red-switch’ for Al³⁺ over ESIP based ‘green-switch’ for Zn²⁺: dual channel detection with live-cell imaging on a dyad platform. *RSC Adv* 2014;4:34572–6.
- [62] Gupta VK, Mergu N, Kumawat LK, Singh AK. A reversible fluorescence “off-on-off” sensor for sequential detection of aluminum and acetate/fluoride ions. *Talanta* 2015;144:80–9.
- [63] Tsui YK, Devaraj S, Yen YP. Azo dyes featuring with nitrobenzoxadiazole (NBD) unit: a new selective chromogenic and fluorogenic sensor for cyanide ion. *Sens Actuators B* 2012;161:510–9.
- [64] Lee SA, You GR, Choi YW, Jo HY, Kim AR, Noh I, et al. A new multifunctional Schiff base as a fluorescence sensor for Al³⁺ and a colorimetric sensor for CN⁻ in aqueous media; an application to bioimaging. *Dalton Trans* 2014;43:6650–9.
- [65] Ding W-H, Wang D, Zheng X-J, Ding W-J, Zheng J-Q, Mu W-H, et al. A turn-on fluorescence chemosensor for Al³⁺, F⁻ and CN⁻ ions, and its application in cell imaging. *Sens Actuators B* 2015;209:359–67.
- [66] Chowdhury AR, Ghosh P, Roy BG, Mukhopadhyay SK, Murmu NC, Banerjee P. Cell permeable fluorescent colorimetric Schiff base chemoreceptor for detecting F⁻ in aqueous solvent. *Sens Actuators B* 2015;220:347–55.
- [67] Sharma D, Moirangthem A, Roy SM, Kumar ASK, Nandre JP, Patil UD, et al. Bioimaging application of a novel anion selective chemosensor derived from vitamin B6 cofactor. *J Photochem Photobiol B* 2015;148:37–42.
- [68] Mahapatra AK, Maji R, Maiti K, Adhikari SS, Mukhopadhyay CD, Mandal D. Ratiometric sensing of fluoride and acetate anions based on a BODIPY-azaindole platform and its application to living cell imaging. *Analyst* 2014;139:309–17.

- [69] Xu S-Y, Sun X, Ge H, Arrowsmith RL, Fossey JS, Pascu SI, et al. Synthesis and evaluation of a boronate-tagged 1,8-naphthalimide probe for fluoride recognition. *Org Biomol Chem* 2015;13:4143–8.
- [70] Ghosh P, Roy BG, Mukhopadhyay SK, Banerjee P. Recognition of fluoride anions at low ppm level inside living cells and from fluorosis affected tooth and saliva samples. *RSC Adv* 2015;5:27387–92.
- [71] Sivaraman G, Chellappa D. Rhodamine based sensor for naked-eye detection and live cell imaging of fluoride ions. *J Mater Chem B* 2013;1:5768–72.
- [72] WHO (World Health Organization). Guidelines for drinking-water quality. 4th ed. 2011. p. 1–564.
- [73] Chaumont FD, Dallongeville S, Chenouard N, Hervé N, Pop S, Provoost T, et al. Icy: an open bioimage informatics platform for extended reproducible research. *Nat Methods* 2012;9:690–6.
- [74] Ding W-H, Wang D, Zheng X-J, Ding W-J, Zheng J-Q, Mu W-H, et al. A turn-on fluorescence chemosensor for Al^{3+} , F^- and CN^- ions, and its application in cell imaging. *Sens Actuators B* 2015;209:359–67.